Energy Conversion and Management 171 (2018) 576–586

Contents lists available at ScienceDirect

Energy Conversion and Management

journal homepage: www.elsevier.com/locate/enconman

Energy efficient multi-effect distillation powered by a solar linear Fresnel collector

Mohamed Alhaj[a], Abdelnasser Mabrouk[a,b], Sami G. Al-Ghamdi[a,*]

[a] Division of Sustainable Development, College of Science and Engineering, Hamad Bin Khalifa University, Qatar Foundation, Doha, Qatar
[b] Qatar Environment and Energy Research Institute, Hamad Bin Khalifa University, Qatar Foundation, Doha, Qatar

ARTICLE INFO

Keywords:
Multi-effect distillation (MED)
Thermal vapor compression (TVC)
Solar desalination
Linear Fresnel collector (LFC)
Air-cooled condenser

ABSTRACT

Solar-driven desalination is a potential solution to the problem of freshwater scarcity in many parts of the world. However, this technology requires considerable efforts to overcome a number of technical challenges such as high-energy consumption, intermittency of solar radiation, and high-water consumption. This paper proposes an optimized multi-effect distillation (MED) process driven by steam at 70 °C and 0.3 bar, which is provided by a linear Fresnel collector. The aim of the proposed integrated system is to reduce the equivalent mechanical energy of the MED process, and utilize the most cost-effective storage system. Moreover, we incorporated an air-cooled condenser instead of a water-cooled condenser, to reduce the water cooling facilities. A computer model was developed using the Engineering Equation Solver tool, to solve the mass and energy balance equations of the integrated system (under different operating conditions). Under the operating conditions of Qatar, the simulation results showed that 1 m^2 of solar linear Fresnel collector produces 8.6 m^3 of freshwater per year. The equivalent mechanical energy of the optimized MED desalination plant is 8 kWh/m^3, which is 59% lower than that of existing commercial MED facilities with thermal vapor compression (19 kWh/m^3). This significant reduction in equivalent energy consumption would reduce the required solar field size by 25%. This study also showed that using a water storage system (instead of thermal energy storage) results in a lower total system capital cost. Furthermore, by integrating an air-cooled condenser, the overall plant water consumption reduced by 2 m^3 of sea water per m^3 of feed water. The performance of the air-cooled condenser can vary by as much as 300% due to fluctuations in dry-bulb temperature and relative humidity.

1. Introduction

Water scarcity in many regions around the world means that reliance on desalination technologies is imminent. In the Gulf Cooperation Council (GCC) countries, 80% of drinking water comes from desalination plants [1,2]. In fact, 38% of global desalination capacity is in the GCC region [3]. Thermal desalination, including multi-stage flash (MSF), multi-effect distillation (MED), and MED with thermal vapor compression (MED-TVC) technologies dominate the desalination industry in the GCC countries. Furthermore, the reverse osmosis (RO) membrane technology market is also growing, owing to its high energy efficiency [4]. The harsh gulf seawater conditions (high temperature, high salinity, high impurity, and sometimes red tide) make the use of thermal desalination technology a reliable solution [5]. Thermal desalination processes (such as MSF and MED) are also preferred in the GCC region due to their robustness [6]. Among the thermal desalination technologies, MED operates at a lower specific power consumption (SPC) than the MSF process. This is a result of using falling film evaporation around the tubes (three times the distillate) instead of pumping a bulk flow of seawater feed (ten times the product) [7]. A techno-economic analysis showed that plain MED desalination technology delivers a lower unit water cost compared with existing MSF and MED-TVC technologies [8]. This is because plain MED uses a low steam pressure of 0.3 bar at 70 °C, which is lower than MSF and MED-TVC (3 bar at 180 °C).

The demand for freshwater is rising because of population increase, and this will further magnify the problem of freshwater scarcity [9]. This will increase pressure on current desalination plants and require more plants to be built, which will in turn escalate energy and fuel demands. These factors will also lead to a greater impact on the environment. Solar-driven desalination is a potential solution to this problem.

The coupling of solar power technologies with desalination is an interesting area of research, but requires further development and improvement [10]. Among the currently developed solar desalination technologies, the solar-driven MED process is possibly the most suitable

* Corresponding author.
E-mail address: salghamdi@hbku.edu.qa (S.G. Al-Ghamdi).

https://doi.org/10.1016/j.enconman.2018.05.082
Received 14 March 2018; Received in revised form 14 May 2018; Accepted 21 May 2018

Nomenclature

η_{fan}	fan electric efficiency
$\eta_{optical}$	optical efficiency
ΔP	condenser pressure change
A	aperture area (m^2)
$A_{specific}$	specific area (m^2/kg/s)
CSP	concentrated solar power
DHI	diffuse horizontal irradiance (W/m^2)
DNI	direct normal irradiance (W/m^2)
EES	engineering Equation Solver
GHI	global horizontal irradiance (W/m^2)
GOR	gain output ratio
HTF	heat transfer fluid
LFC	linear Fresnel collector
$L_{receiver}$	receiver length (m)
MED	multi-effect distillation
MR	mixing ratio
MSF	multi-stage flash
PTC	parabolic trough collector
Q_{field}	solar field power (kW)
Q_{loss}	thermal losses (kW)
RO	reverse osmosis
SAM	system Adviser Model
SPC	specific power consumption (kWh/m^3)
T_1	HTF inflow temperature (C)
T_2	HTF outflow temperature (C)
TES	thermal energy storage
$T_{receiver}$	receiver temperature (C)
TVC	thermal vapor compressor
V_{air}	air volumetric flow rate
W_{fan}	fan power

for large-scale implementation. This is because of its superior thermodynamic and heat transfer performance (compared to the MSF process), and lower levelized cost of water [11,12]. The MED process generally has a lower energy consumption rate than the MSF process.

Generally, research into solar-driven MED and solar desalination is still in its early phases, with many critical problems remaining unsolved [13].

The Plataforma Solar de Almeria plant (Spain) is one of the earliest solar-driven thermal desalination pilot plants. This plant used compound parabolic collectors, a 14-effect vertical stack MED configuration, with an absorption heat pump. Results showed that the heat consumption of the plant could be optimized by using a heat pump [14]. The Abu Dhabi solar desalination plant is also among the earliest of the pilot plants [15]. The plant used flat plate collectors, a 14-effect MED system, and a thermal storage system that facilitated 24 h operation. The distillate production was 120 m^3/day, and the water cost was 7–10 $ per m^3.

Sharaf et al. [16] carried out a thermo-economic analysis for two configurations of a solar-driven MED plant (both with and without a TVC), and considered the cogeneration of desalted water and electric power in both cases. The study found that solely producing desalted water is better than cogeneration in terms of water cost and solar field area. Hamed et al. [17] conducted an experimental study to characterize the thermal and optical performance of a new linear Fresnel collector (LFC) that can supply heat to a MED-TVC plant. The study used oil as the heat transfer fluid (HTF), with an inlet temperature of 100 °C and an outlet temperature of 300 °C. The LFC had a peak optical efficiency of 67%, which is slightly higher than other similar commercial systems. The coupling of the solar collector to the MED-TVC plant was simulated under a scenario where the LFC provided 20% of the thermal requirements of the MED-TVC unit. Based on this, it was found that to produce a thermal energy of 13.6 MW_{th} to power the MED-TVC unit, a solar field area of 55,737 m^2 was required. The authors suggested setting the outlet temperature of the HTF to a low value, to increase the thermal efficiency of the solar field. Askari and Ameri [13] conducted a simulation study in which the performance of an LFC solar field coupled to an MED plant was modeled, using MATLAB and the System Advisor Model (SAM) software. This hybridized system incorporated a natural gas boiler and a thermal energy storage (TES) tank. The authors performed a detailed techno-economic analysis of the plant under different scenarios, in which the system scale was modified. Results showed that the minimum water cost was obtained at the lowest solar share (27.54%). In addition, if the TES system cost is more than $100/kWh, then using a water storage system is more economical. Furthermore, the authors highlighted the fact that solar thermal energy is still very expensive as a replacement for conventional desalination energy.

Iaquaniello et al. [18] carried out a technical and economic analysis on an MED-RO plant that produces electricity and desalted water, and is powered by solar heat from a parabolic trough collector (PTC). The simulations in their study were based on a robust computer model. Their hybrid configuration resulted in a water cost of less than $1.23/$m^3$. It was found that increasing the plant life from 20 to 30 years reduces the water cost by 8%. Mabrouk et al. [19] presented the design and simulation of an MED system powered by a PTC. The system proposed the use of brine recirculation and an air-cooled condenser. The study found that using an air-cooled condenser reduces the capital cost of groundwater.

A further study experimentally investigated a high-performance MSF desalination unit, integrated with a nano filtration membrane, and driven by a concentrated parabolic collector [20]. The nano filtration pilot was built to enable the MSF desalination unit to operate at high top brine temperature. The capacity of the desalination pilot plant is 1.0 m^3/day of water. This newly developed NF-MSF configuration is tested at a top brine temperature of 100 °C, and the gain output ratio (GOR) is calculated as 15, which is almost twice that of a conventional MSF under the same operating conditions. This newly developed high-performance NF-MSF process (with its lower input thermal energy) makes integration with relatively expensive solar power collectors a viable option.

A critical review by the authors discussed the literature on a solar-driven MED in detail, and highlighted key research gaps that should be addressed [21].

A number of conclusions were derived from the literature. Most studies in the literature considered using the PTC [16,22–26]. The PTC is a commercially mature technology, and has been widely used in power generation for many years. However, it is more expensive (in terms of specific capital cost) than similar concentrating solar power (CSP) collectors, such as the LFC. The specific capital cost for a PTC is 378–430 $/$m^2$, compared to 246–307 $/$m^2$ for an LFC [27]. The LFC could be a better choice for MED as it has a lower concentration factor, which is suitable for an MED process that requires steam at 70 °C and 0.3 bar. The LFC is also more compact and has a smaller mass per m^2, resulting in better land utilization. Some studies on solar-driven MEDs used an LFC in their system [13,17]. The use of LFCs in MED systems needs to be explored in more detail, to fully understand the potential of this solar collector.

A critical review [28] explored thermal and non-thermal storage systems (used with desalination systems), and showed the features of both. The review asserted that the addition of thermal storage to a desalination system can lead to both lower water costs, and better management of the intermittent solar resource. A number of solar-driven desalination studies used a TES in the system design [13,15,17,22,23,25,29,30]. Some studies did not use the TES

[16,24,26,31–33]. Few studies considered the use of phase change materials in a solar desalination system. Phase change materials have operating temperatures of up to 350 °C, which makes them ideal for a process such as MED-TVC that requires superheated steam (at temperatures close to 200 °C). Furthermore, the thermal power discharge process in phase change materials occurs at a constant temperature, making heat transfer to the desalination unit more stable. A number of phase change materials also have very low specific volumes, which reduces storage system size. Extensive reviews on phase change materials can be found in the Refs. [34–36]. This is an interesting area of research, which has not yet been fully investigated. Using water storage systems is another possible alternative. This configuration requires oversizing the desalination system to produce excess water during daytime. The works by Askari and Ameri [13] and Weiner et al. [37] indicate that water storage could be economically more attractive than TES, under certain conditions.

There is a gap in the literature in assessing whether a solar-driven MED is better with or without a thermal vapor compressor, from an energy viewpoint. Moreover, there is a gap in identifying the best operating and design conditions for making solar-driven MEDs competitive with RO systems, in terms of equivalent electrical energy (also known as equivalent mechanical energy). There is also a need to conduct in-depth comparisons between different storage systems that could be coupled to solar desalination systems. Carrying out an extensive analysis could help in exploring the best applications for solar desalination systems.

Based on the above, the problem statement can be expressed as the optimization of solar-driven multi-effect distillation from the perspective of energy and capital costs. Hence, the objectives of this work are:

- Design and carry out performance simulations of a plain MED plant driven by a solar LFC.
- Investigate the performance of the proposed system under the climate conditions of Qatar.
- Carry out a techno-economic comparison of three possible storage systems.
- Reduce water consumption using an air-cooled condenser.

2. Plant description

The proposed solar-driven MED plant is a seven-effect parallel feed plant with feed preheaters, flash boxes, brine recirculation, and an air-cooled condenser. Fig. 1 shows a schematic of the entire plant. The LFC solar field delivers thermal power to the steam generator, which is then transferred to the MED chamber where successive boiling and condensation takes place. The solar field uses pressurized water as the HTF, which remains in single phase. A variable speed pump is integrated in the solar field to ensure a constant HTF outlet temperature. An air-cooled condenser is integrated after the last effect to condense the generated vapor. Furthermore, this plant utilizes a water storage system instead of energy storage. Our system is designed to operate at a constant average solar field power.

2.1. Model development and validation

The main modeling assumptions are as follows:

- All components are operating at steady-state conditions.
- The hourly solar radiation is constant.
- There is no pressure drop in the LFC system piping because of the small scale of the system.
- The evaporators are insulated, hence there is no heat loss to the environment.
- The pressure drops in the demisters are negligible.
- The distillate has zero salinity.

The model for the entire plant was developed in the Engineering Equation Solver (EES) software using energy, mass, and salt balance for the evaporators, preheaters, flash boxes, and end condenser. The complete EES algorithm was composed of 501 equations, which were solved simultaneously using Newton's method (with a residual of 10^{-6}).

2.1.1. Solar radiation data

Atmospheric data used in the model were all measured at Hamad Bin Khalifa University in Doha, Qatar (in 2016). This consisted of solar radiation data (all three components: global horizontal irradiance (GHI), direct normal irradiance (DNI), and diffuse horizontal irradiance (DHI)), dry and wet bulb temperatures, humidity, and wind speed/direction. The DNI was measured using a Kipp and Zonen CHP1 pyroheliometer, with an uncertainty of 2%. Hourly values of DNI were sampled from the ground measurements dataset, and from these we derived relations for the DNI as a function of time for each month of the year (by curve fitting). This was done for simplicity when inputting the solar radiation data to our model. The DNI function approximations for the year (2016) are given in Table 1. These relations are representative of the typical DNI in Qatar, and can be used to assess the hourly performance of solar collectors. The DNI data (measured and approximated) for a typical day in May 2016 are shown in Fig. 2. This figure shows a close match between the derived relation and the real data.

2.1.2. LFC solar field

The specifications of the LFC solar field are given in Table 2. We computed the hourly optical efficiency of the LFC using the SAM

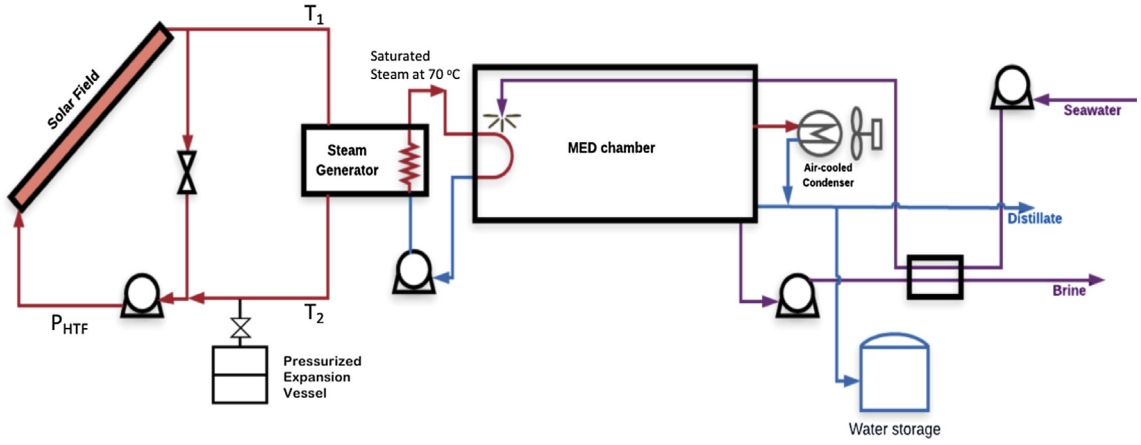

Fig. 1. Schematic of the proposed solar-driven multi-effect distillation plant.

Table 1
DNI function approximations for Doha, Qatar (derived from ground measurements in 2016).

Month	DNI function approximation (W/m^2), for: $5 \le t \le 17$
January	$12217.38 - 8514.11(t) + 2297.42(t^2) - 311.87(t^3) + 23.06(t^4) - 0.89(t^5) + 0.01(t^6)$
February	$12409.00 - 9587.69(t) + 2852.40(t^2) - 420.34(t^3) + 33.17(t^4) - 1.34(t^5) + 0.02(t^6)$
March	$9409.06 - 6716.99(t) + 1836.29(t^2) - 248.40(t^3) + 18.09(t^4) - 0.68(t^5) + 0.01(t^6)$
April	$6223.30 - 4733.62(t) + 1351.50(t^2) - 185.71(t^3) + 13.48(t^4) - 0.50(t^5) + 0.007(t^6)$
May	$5552.56 - 4355.93(t) + 1274.90(t^2) - 178.29(t^3) + 13.09(t^4) - 0.9(t^5) + 0.007(t^6)$
June	$4192.04 - 3286.84(t) + 951.78(t^2) - 130.27(t^3) + 9.34(t^4) - 0.34(t^5) + 0.005(t^6)$
July	$4192.04 - 3286.84(t) + 951.78(t^2) - 130.27(t^3) + 9.34(t^4) - 0.34(t^5) + 0.005(t^6)$
August	$9321.27 - 6861.42(t) + 1933.04(t^2) - 268.15(t^3) + 19.84(t^4) - 0.75(t^5) + 0.011(t^6)$
September	$9606.11 - 7095.61(t) + 2002.73(t^2) - 278.32(t^3) + 20.72(t^4) - 0.80(t^5) + 0.01(t^6)$
October	$16992.09 - 12554.16(t) + 3580.54(t^2) - 507.81(t^3) + 38.58(t^4) - 1.50(t^5) + 0.02(t^6)$
November	$12956.78 - 9304.82(t) + 2585.45(t^2) - 359.54(t^3) + 27.02(t^4) - 1.05(t^5) + 0.01(t^6)$
December	$11727.82 - 8299.30(t) + 2279.40(t^2) - 315.11(t^3) + 23.70(t^4) - 0.92(t^5) + 0.01(t^6)$

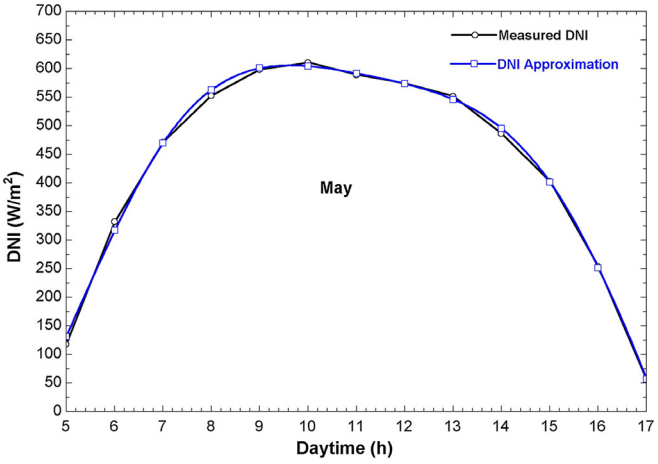

Fig. 2. Measured DNI and function approximation for a typical day in May in 2016 in Doha, Qatar.

Table 2
Technical data of the chosen LFC solar field [38].

Parameter	Value
Field aperture	$8 \times 22 = 176\ m^2$
Absorber tube	SCHOTT PTR® 70
Total absorber length	64.96 m
Absorber diameter	3.47 cm
Max. optical efficiency	66%

software, based on the incidence angle modifier method. The transversal and longitudinal incidence angles for this LFC were given by the manufacturer.

The hourly field power (Q_{field} in kW) is given by

$$Q_{field} = (DNI \times A \times \eta_{optical}) - Q_{loss} \quad (1)$$

where A is the LFC aperture area (m^2), and Q_{loss} is the total thermal loss from the receiver (kW) that is a function of the average temperature of the receiver (°C), given by

$$T_{receiver} = \frac{T_1 + T_2}{2} + 10 \quad (2)$$

where T_1 and T_2 are the inflow and outflow temperatures of the HTF (shown in Fig. 1). Given the value of $T_{receiver}$, Q_{loss} can be estimated based on [39]:

$$Q_{loss} = 8.56993 \times \exp^{(0.00844872 \times T_{receiver})} \times L_{receiver} \quad (3)$$

The design temperature increase in the solar collector was set as 10 °C. Given the design ΔT, the mass flow rate of the HTF could be determined every hour.

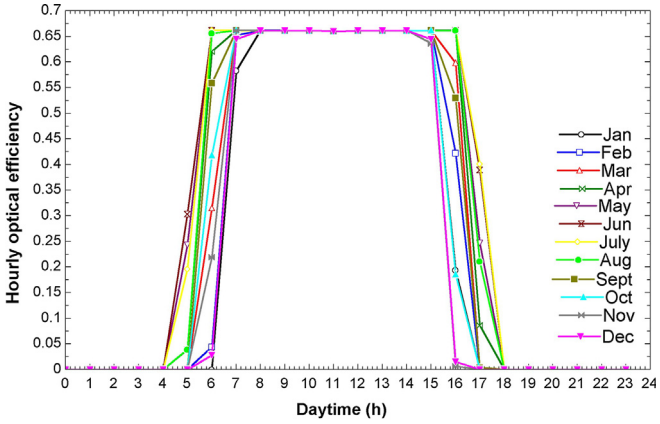

Fig. 3. Hourly optical efficiency for the LFC.

The hourly optical efficiency of the LFC is shown in Fig. 3. It can be observed that the LFC operated at peak optical efficiency (0.66) for almost the entire solar day. Hence, a constant optical efficiency can be assumed when calculating the hourly field power. This also conforms to the specifications of the LFC manufacturer, which states that the optical efficiency is independent of the incidence angle.

The temperature increase across the LFC was set as 10 °C, which is the difference between the inflow and outflow HTF temperatures (pressurized water). The LFC field power (Q_{field}) calculated by our model was validated by comparing it with results given by the manufacturer. Two days were selected for validation (March 25 and April 5), and the results are shown in Figs. 4 and 5. The error between the model and manufacturer data is given in Table 3. The maximum absolute error

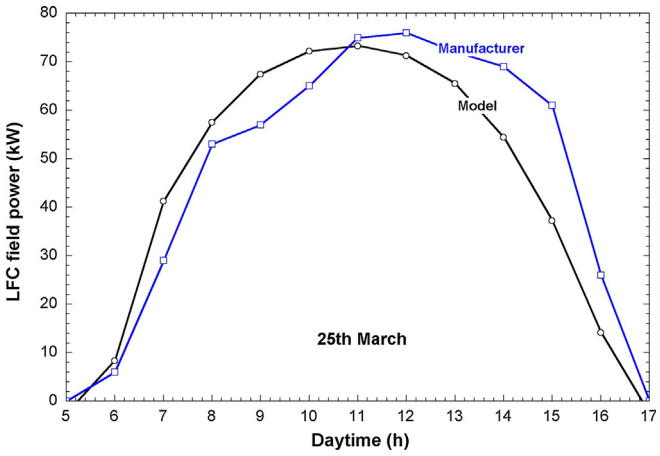

Fig. 4. LFC field power in March 25, 2016.

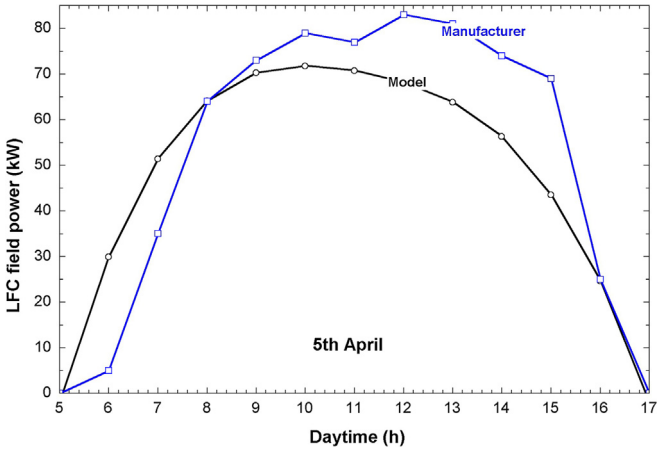

Fig. 5. LFC field power in April 5, 2016.

Table 3
Solar field model validation.

Month	Model's results – average field power (kW)	Manufacturer's results – average field power (kW)	Absolute error (%)
March	42.9	45.3	5.3
April	47.1	51.2	8

was 8%, which demonstrates that the developed model is acceptable.

Fig. 6 shows the hourly field power and thermal losses for the month of May. It can be observed that the field power follows the same bell-shaped profile of the DNI, and the thermal losses are very small compared to the hourly field power. This shows that most of the incident solar energy absorbed by the receiver is transferred to the HTF. The average power line indicates the power delivered to the MED plant section during daytime. The desalination system was only operational during solar hours, when the LFC field power is greater than or equal to the average power.

2.1.3. MED model

The MED model was developed using energy, mass, and salt-balance relations. The relations given by El-Dessouky and Ettouney [40] were used to calculate the overall heat transfer coefficient in the evaporators, preheaters, and end condenser. The sea water properties (specific heat capacity and density) were evaluated as a function of temperature and salinity, using the Sea Water Properties library in EES [41,42]. The MED model was validated by comparing it with a commercial MED plant that has a productivity of 1137 ton/h (located in the GCC region). The chosen plant uses MED-TVC, therefore our model relations also need to include a simulation of the performance of the thermal vapor compressor. The relations given by Hassan and Darwish [43] were used to calculate the mixing ratio for the TVC, given the motive steam pressure, entrained vapor pressure, discharge pressure, and mass flow rate of the motive steam. The validation results are presented in Table 4. It can be observed that our model outputs were all within 5% absolute error, proving the reliability of the model.

2.1.4. Plant performance metrics

The main performance metrics for this system were GOR, SPC, specific area (A_{spec}), specific thermal power, and productivity.

The specific thermal power is given by:

$$\text{Specific thermal power} = \frac{\text{Average solar field power}}{\text{Plant productivity}} \quad (4)$$

3. Results and discussion

3.1. Simulation of the solar-driven conventional MED-TVC system under Qatar's climate

The first set of results represents the expected performance of the solar-driven conventional MED-TVC plant. This configuration is common, and hence marks the baseline for our optimization studies, which are presented in the next section. Table 5 presents the entire plant specifications and performance results, which are appropriate for the small solar field size given in Table 2. Inputs are marked with a superscript (i) and outputs are marked with a superscript (o).

Table 5 reflects the expected performance of a small-scale solar desalination plant located in Qatar. Given a solar field aperture area of 176 m^2, the desalination system produced 734 kg of freshwater per hour. This is equivalent to 4.2 kg/h of freshwater produced per m^2 of solar LFC under Qatar's climate conditions. The table indicates that this plant consumed 19 kWh/m^3 of equivalent mechanical energy, which is close to values reported in the literature for high pressure MEDs [44]. The specific thermal energy value of 81.7 kWh/m^3 obtained from our model is comparable to values reported in the literature. For example, 87.9 kWh/m^3 was reported by Sharaf et al. [31], and 71.8 kWh/m^3 was reported by Hamed et al. [17]. In the next sections we present details on the optimization of the conventional system, by focusing on the investigation of equivalent mechanical power, storage system selection, and integration of an air-cooled condenser.

3.2. Investigation of equivalent mechanical power

Table 5 indicates that the equivalent mechanical energy was 19 kWh/m^3, which is much higher than RO systems where mechanical energy consumption is in the range of 5–7 kWh/m^3. To reduce this value for thermal desalination systems, the number of effects must be increased. Fig. 7 shows the equivalent mechanical energy for thermal desalination systems, as a function of steam pressure and GOR. In every iteration, the GOR and productivity (1 m^3/h) were fixed. The feed mass flow rate and the number of effects were varied automatically to achieve the design GOR. The steam pressure was varied from 0.25 bar up to 5 bar. The figure shows that the equivalent mechanical energy drastically reduced as the steam pressure reduced. Furthermore, by increasing the GOR, the equivalent mechanical energy also reduced. As the number of evaporators increases, more generated vapor is reused within the plant, which reduces the external heat requirements. Hence, the equivalent mechanical energy reduces. An important conclusion from Fig. 7 is that removing the thermal vapor compressor resulted in reduced thermal energy consumption. The conventional design point (steam pressure = 3 bar), and the optimal design point (steam

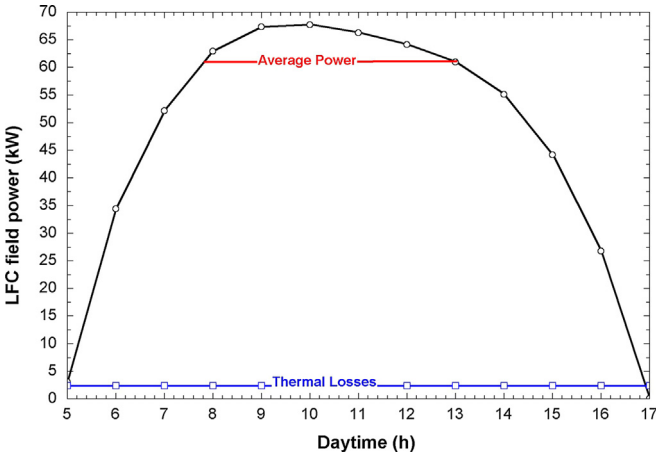

Fig. 6. Hourly LFC power, average power, and thermal losses (month of May).

Table 4
MED model validation.

Parameter	Real	Model	Absolute error (%)
Number of effects	7	7	–
Heating steam temperature in first effect (°C)	68	68	–
Sea water temperature (°C)	35	35	–
Sea water salinity (g/kg)	48	48	–
Motive steam pressure (bar)	2.4	2.4	–
TVC discharge pressure (bar)	0.285	0.285	–
Entrained vapor pressure (bar)	0.161	0.161	–
Gain output ratio	9.07	8.90	1.87
Top brine temperature (°C)	66.00	65.49	0.77
Brine temperature in last effect (°C)	44.10	43.61	1.11
Effect 1 brine salinity (g/kg)	70.40	73.69	4.67
Last effect brine salinity (g/kg)	69	68.43	0.8
Temperature of condenser reject water (°C)	41.00	40.85	0.37

Table 5
Solar-driven conventional MED-TVC plant specifications and simulation results from our model.

Parameter	Value
TVC	
[i]Motive steam pressure (bar)	3
[i]Discharge steam pressure (bar)	0.3
[o]Discharge steam temperature (°C)	70
[i]Entrained vapor pressure (bar)	0.07
[o]Compression ratio	4.385
[o]Mixing ratio	2.99
MED chamber	
[i]Number of effects	7
[i]Top brine temperature (°C)	65
[i]Feed mass flow rate (kg/h)	2520
Feed type	Parallel flow
[i]Seawater temperature (°C)	30
[i]Seawater salinity (g/kg)	48.2
[o]Seawater intake (kg/h)	8400
[i]Design ΔT in end condenser (°C)	7
[i]Brine temperature in the last effect (°C)	40
Performance results	
GOR	8.3
Specific thermal power (kWh/m^3)	81.7
Specific power consumption (kWh/m^3)	2.1
Equivalent mechanical energy (kWh/m^3)	19.2
Specific area (m^2/kg/s)	282
Productivity (kg/h)	734
Brine disposal temperature (°C)	38
Brine disposal salinity (g/kg)	52.8

pressure = 0.3 bar), are also marked in Fig. 7. Fig. 8 shows the equivalent mechanical energy for different numbers of evaporators. As expected, increasing the number of evaporators reduced the equivalent mechanical energy consumption, because of more thermal energy recovery within the desalination system.

Based on the above findings, we made a comparison between an MED system (with TVC) and a low-pressure MED system (without TVC), which have the same productivity of 1 m^3/h.

Table 6 presents the results of this comparison. The table indicates that in the low-pressure MED configuration, the equivalent mechanical energy is 59% less than the MED-TVC configuration. The equivalent mechanical energy in the low-pressure MED system is comparable to RO systems. This proves the possibility of thermal desalination competing with RO systems, from an energy viewpoint. The reduced energy consumption is also reflected in the reduced solar field aperture area (approximately 25% less than an MED-TVC system). This is critical for a solar desalination system, where the solar field is usually the highest capital cost contributor. The solar field area is lower because of the larger number of effects in the low-pressure MED system. This results in a greater reusability of the generated vapor, and hence lower external heat requirements. The only disadvantage in the low-pressure MED configuration is the large number of evaporators, which resulted in a 128% increase in evaporator surface area compared with the MED-TVC configuration.

The distinguishing features of using the low-pressure MED configuration over MED-TVC (in solar-driven desalination systems) can be summarized as follows:

- Less equivalent mechanical energy consumption, but a larger number of evaporators.
- Lower steam pressure and temperature, which means that low concentrating collectors can be used, resulting in cheaper specific cost.
- Lower operational costs, but higher capital costs in the desalination sub-section.
- Lower capital and operational costs in the solar field subsection (a reduced aperture area results in a smaller solar field size).
- In the case of a single-phase HTF in the solar field, the solar field can be operated at a low pressure because no high-pressure motive steam is required. This results in increased plant reliability.

A sensitivity analysis was performed to compare the effect of increasing the number of evaporators on the LFC field area and the MED evaporator area (for the low-pressure MED configuration). Fig. 9 shows the results of this analysis. As expected, increasing the number of evaporators increased the total MED area, but reduced the required LFC aperture area. Increasing the number of evaporators from 7 to 16 increased the MED heat transfer area by more than 4 times, whereas the LFC aperture area reduced by only 50%. This shows that the MED heat transfer area is more sensitive to the number of evaporators than the LFC aperture area. However, in terms of cost, 1 m^2 of solar field is not the same as 1 m^2 of desalination system. The optimum number of effects is 10, because this will result in a reasonable temperature difference per effect (approximately 2 °C). At 10 evaporators, the LFC aperture required to produce 1 m^3/h of distillate was 226 m^2, and the equivalent mechanical energy consumed was 8 kWh/m^3. The specifications of the optimized solar-driven MED plant are given in Table 7.

3.3. Storage system techno-economic optimization

As highlighted in the literature review earlier, selecting the best storage system for solar desalination plants is an important area of research. There are two possible storage systems that could be coupled to the desalination processes: TES and water storage. Thermal energy storage could be based on sensible or latent heat materials. The storage system stores excess thermal energy (from the solar field) during daytime, and uses it to extend the operational period of the plant after sunset. Water storage means oversizing the solar field to produce excess water during the day, which is then transported to consumers at night. A water storage-based solar desalination system operates at a higher rate than using TES. The optimal selection of the storage system depends on capital costs and storage volume. We carried out a general comparison between three categories of storage: sensible heat storage, latent heat storage, and water storage systems. The goal of this analysis is to compare the capital costs and storage system volume for these three categories. The storage systems selected were molten salt (sensible heat storage), potassium chloride-lithium nitrate (KCl-$LiNO_3$, latent heat storage), and a simple water tank for the water storage system. The chosen storage systems alongside their corresponding energy density and specific cost are shown in Table 8. The independent variable in this comparison was a daily plant production of 13 m^3 of freshwater. The dependent variables were storage system volume and total plant capital costs. When using sensible and latent heat systems, the solar field must be oversized to ensure that enough excess energy is available for the storage system. The corresponding solar field sizes,

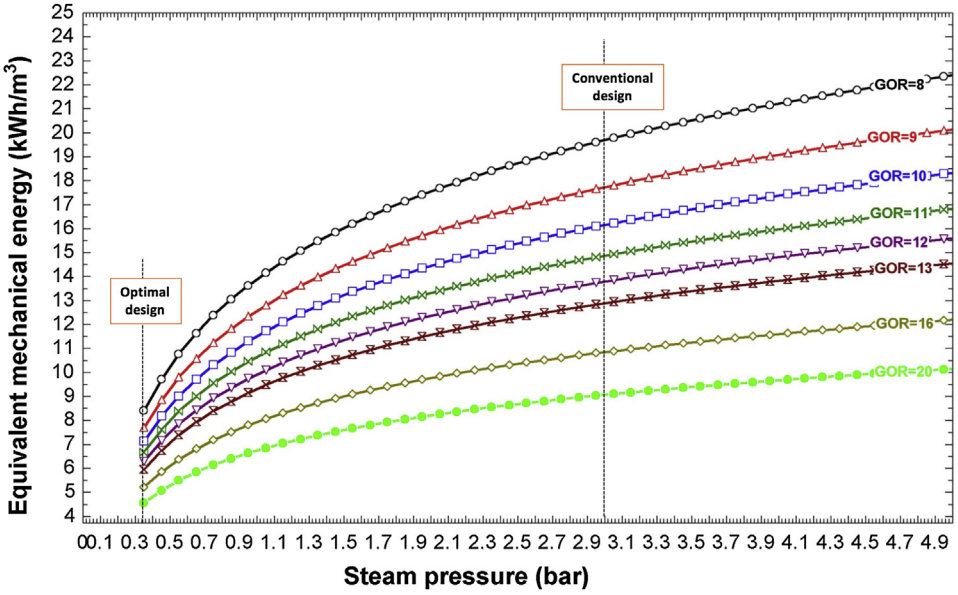

Fig. 7. Equivalent mechanical energy at different steam pressures and GOR.

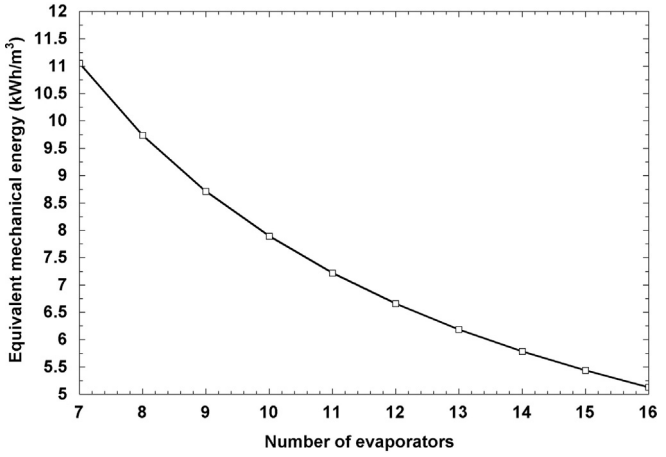

Fig. 8. Equivalent mechanical energy as a function of number of evaporators.

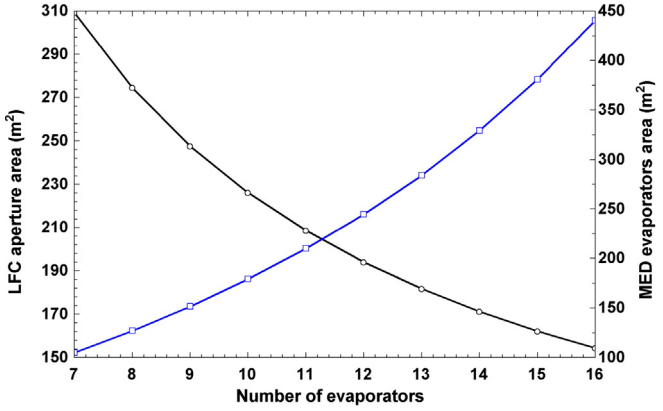

Fig. 9. LFC aperture area and MED evaporator area as a function of number of evaporators.

Table 6
Comparison of MED-TVC with low-pressure MED for a fixed distillate production.

Parameter	MED-TVC	Low-pressure MED
Productivity, m^3/h	1	1
GOR	8.3	8.3
Number of evaporators	7	10
Maximum steam pressure (bar)	3	0.3
Steam temperature in first effect (°C)	70	70
Equivalent mechanical energy (kWh/m^3)	19.1	7.9
Evaporators area (m^2)	78.3	179.3
LFC aperture area (m^2)	300	226

MED evaporator areas, and storage system volumes were calculated and are presented in Table 9. This table indicates that the latent heat storage system has the smallest volume owing to the higher volumetric energy density, which is common in PCMs. In all three cases, the solar field size had to be increased by 50% and 39% for the energy storage and water storage systems, respectively. This increase is relative to the original solar field size of 226 m^2 (refer to Table 7), where no storage was considered. The incorporation of the storage system increased the plant daily productivity by 62%, form an initial daily production of 8–13 m^3.

Table 7
Specifications of the optimized solar-driven MED plant.

Parameter	Value
Solar field aperture area, m^2	226
Temperature drop in the steam generators, °C	10
Number of evaporators	10
Distillate production, m^3/h	1
Plant annual yield, m^3 of freshwater/m^2 of solar LFC	8.4
Equivalent mechanical energy, kWh/m^3	7.9

Table 8
Possible storage systems for coupling with a solar-driven desalination plant.

Storage system	Energy density	Specific cost	Refs.
Sensible heat storage	0.76 kWh/m^3·C	$30/kWh	[28,45]
Latent heat storage	201.7 kJ/kg	$50/kWh	[34,46]
Water storage	4.2 kJ/kg·C	$0.25/L	–

By considering representative cost values for the MED system and the solar field [13], we calculated a simplified total plant capital cost for the three storage systems. The capital cost breakdowns are shown in Fig. 10. These costs represent a solar-driven MED plant located in Qatar

Table 9
Solar field size, MED evaporator area, and storage system volume for three storage options.

Storage system	Required solar field size (m^2)	Required MED evaporator area (m^2)	Storage system volume (m^3)	Daily freshwater production (m^3)	Night-time operation (h)
Sensible heat storage	338.9	125.4	4.9	13	5
Latent heat storage	338.9	125.4	3.3	13	5
Water storage	314.6	181.2	4	13	0

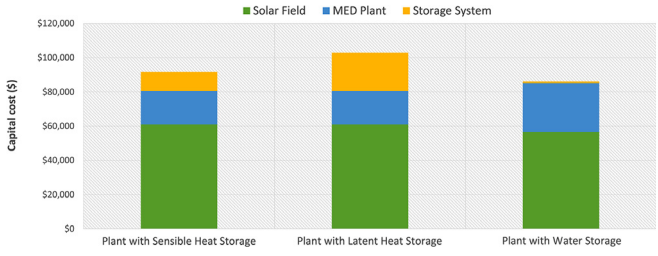

Fig. 10. Comparative total plant costs for three configurations of a solar-driven MED plant with a capacity of 13 m^3/day.

with a capacity of 13 m^3 per day. All the bars in Fig. 10 indicate that most of the plant costs are from the solar field (at least 60%). This implies that cost reductions in the solar field would have the highest influence on total system cost. The results of the analysis by Askari and Ameri [13] also revealed a high solar field capital cost share; 75% of the total plant capital costs. Fig. 10 shows that 12% of the total system cost (for the plant with sensible heat storage) was from the sensible heat storage system, whereas in the case of the latent heat storage this value was 22%. This is attributed to the low commercial maturity of latent heat storage systems in the market, which causes their specific costs to be higher (even though they have a higher energy density). Furthermore, latent heat storage systems such as KCl-LiNO3 contain toxic materials, and hence require high levels of safety. Fig. 10 shows that the water storage system has negligible costs, because it is simply a tank. By comparing the capital costs of the three systems, the capital costs for the plant with water storage system is 6% lower than the plant with sensible heat storage, and 16% lower than the plant with latent heat storage system. This shows that from a capital expenditure and plant operation perspective, water storage systems are more economical than energy storage systems.

3.4. Air-cooled condenser integration

The common practice in thermal desalination processes is to use a water-cooled condenser for condensing the vapor generated in the last effect, and also to preheat the feedwater. However, these condensers consume large amounts of sea water (approximately two-thirds of the intake seawater is rejected and returned to the sea). In addition, they consume a lot of electrical pumping power. Using an air-cooled condenser is a good alternative, particularly in areas with low water availability. Air-cooled condensers require a larger heat transfer area because of the small overall heat transfer coefficient. However, they consume zero water, and are therefore highly suitable for applications in remote areas.

We modified the conventional plant design to include an air-cooled condenser, instead of a water-cooled condenser. We selected an air-cooled condenser based on the A-frame configuration and being constructed from galvanized steel [19]. In this configuration, saturated vapor from the last effect enters two finned tubes (shaped like an A-frame). An axial fan blows air across these tubes, which causes condensation. The fan power consumption was calculated under the average dry bulb temperature and relative humidity for Doha in May ($T_{dry\ bulb}$ = 31.9 °C, relative humidity = 0.45) [47]. The fan electrical power is given by:

$$W_{fan} = \frac{V_{air} \times \Delta P}{\eta_{fan}} \quad (5)$$

where V_{air} is the air volumetric flow rate (m^3/s), ΔP is the pressure increase (kPa), and η_{fan} is the fan efficiency (0.9). The air density was calculated in EES, using the relations given by Hyland and Wexler for moist air [48]. The pressure increase is given by the empirical relation reported by Heyns [49]:

$$\Delta P = 320.0451719 - 0.2975215484 \times V_{air} + 6.351486 \times (10^{-4}) \times (V_{air}^2) \times -8.14(10^{-7}) \times (V_{air}^3) \quad (6)$$

Given the above, a comparison was made between a conventional water-cooled condenser and an air-cooled condenser, for the same plant capacity. The results are shown in Table 10. The table indicates that the air-cooled condenser had water savings equivalent to 2 m^3 of seawater for every 1 m^3 of feed water. The electrical energy consumption of the air-cooled condenser was slightly higher than the water-cooled condenser. This is attributed to the high ambient air temperature in May, which led to a higher air volumetric rate. This result represents the worst-case scenario. The area of air-cooled condenser corresponding to this scenario is 6.6 m^2. When the model was run for the month of January ($T_{dry\ bulb}$ = 17.4 °C, relative humidity = 0.74), the plant SPC reduced from 2.5 to 1.5 kWh/m^3. This highlights the sensitivity of the performance of the air-cooled condenser to air conditions. Further, we observed that in order to reduce the air volumetric flow rate, the brine temperature in the last effect had to be increased from the base value of 40–45 °C. This was to increase the overall logarithmic mean temperature difference across the condenser, and as a result reduce the mass flow rate.

We also carried out a number of parametric studies to investigate the performance of the air-cooled condenser. We examined the effect of sea water temperature, solar field aperture area, and ambient air conditions on the electrical power consumption of the condenser. For the first study, we varied the sea water temperature from 20 to 35 °C, and calculated the fan power under different GORs. The results are shown in Fig. 11. We can observe from this figure that an increase in the GOR resulted in lower fan power. This is because the generated vapor is reused within the large number evaporators to produce more vapor, reducing the amount of saturated vapor in the last effect. This results in a lower thermal load for the condenser, and therefore lower pumping energy. As the sea water temperature reduced, the plant productivity decreased (as more latent heat is used for preheating). A decrease in plant productivity reduces the thermal load of the condenser. Given a sea water temperature of 30 °C, increasing the GOR from 7 (i.e., 8 effects) to 12 (i.e., 15 effects) reduced the fan power by 21%. For the second study, the fan power was calculated for three solar field sizes: 113 m^2 (half the base size), 226 m^2 (base size), and 452 m^2 (double the

Table 10
Comparison of the water-cooled and the air-cooled condensers.

Parameter|System	Water-cooled condenser	Air-cooled condenser
Plant specific electric power consumption (kWh/m^3)	2.1	2.5
Water savings (m^3 of seawater/m^3 of feed)	0	2

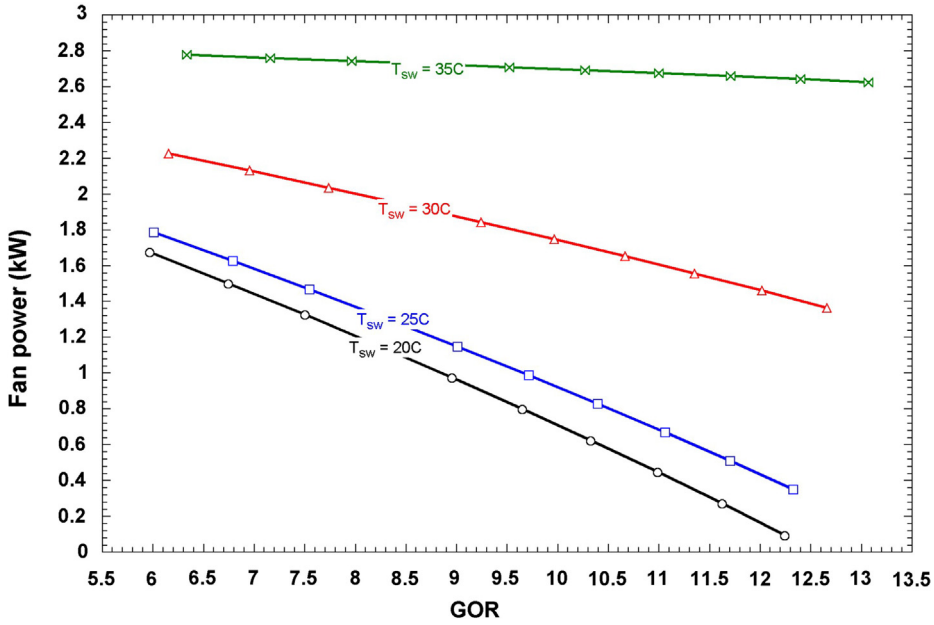

Fig. 11. Fan power under variable sea water temperatures.

base size). The results are given in Fig. 12. It can be clearly observed that as the aperture area increased, the fan power increased. This is due to the increase in vapor produced in the last effect. This figure also shows that doubling the aperture area also doubled the fan power. By comparing Figs. 11 and 12, we can deduce that the fan power is more sensitive to sea water temperature than to solar field size. The third study examined the plant performance under variable air conditions. The long term average monthly air dry bulb temperature and relative humidity in Qatar (taken from the Qatar Meteorological Department webpage) were used as inputs, and the equivalent fan power for each month was calculated. The results are shown in Table 11. We can observe that the relative humidity is inversely related to the dry bulb temperature. The high ambient air temperature during the period (April–September) resulted in a very high fan power, due to the small temperature differential between ambient air and the saturated vapor from the last effect. The variation of fan power reached 300% between some months. The above results indicate the necessity for accurate condenser design to ensure flexibility during operation.

4. Conclusion

Solar-driven desalination is a promising technology for tackling the global challenge of freshwater scarcity. However, this technology requires extensive research to both improve the process energy efficiency and reduce capital expenditures. In this work, a computer program was developed to simulate the performance of (and optimize) an integrated multi-effect distillation plant, driven by a solar linear Fresnel collector. The developed model was validated against real MED plants, with a maximum error of 8%. A number of parametric studies were carried out on the proposed system. We investigated the effect on the overall plant

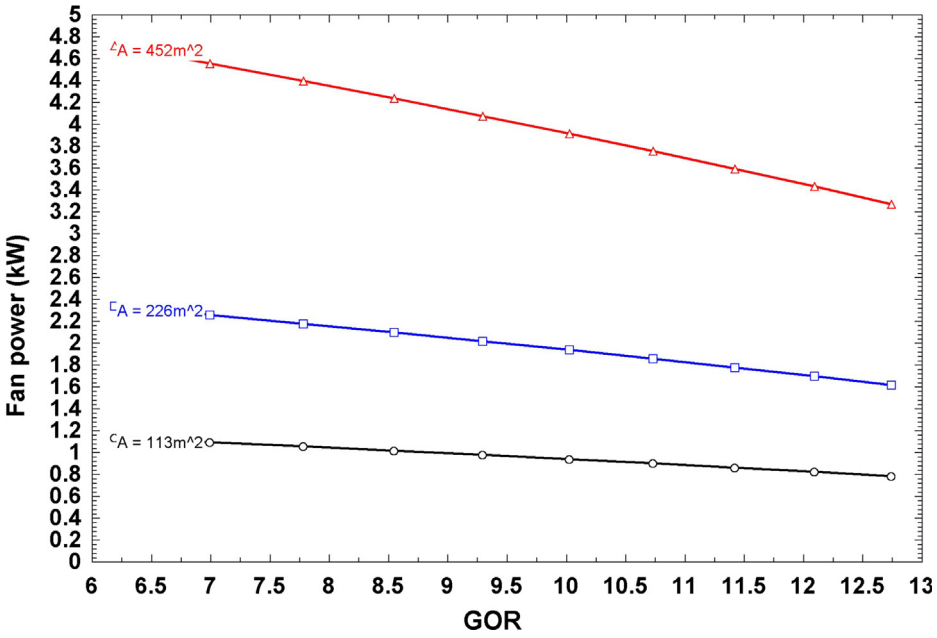

Fig. 12. Fan power under variable solar field aperture areas.

Table 11
Monthly dry-bulb temperature, relative humidity, and calculated fan power.

Month	Jan	Feb	Mar	Apr	May	Jun	Jul	Aug	Sep	Oct	Nov	Dec
$T_{dry\ bulb}$ (°C)	17.4	18.6	21.8	26.4	31.9	34.4	35.3	34.9	32.8	29.6	24.6	19.6
Relative humidity	0.74	0.71	0.63	0.55	0.45	0.45	0.50	0.61	0.62	0.65	0.68	0.74
Fan power (kW)	0.75	0.84	0.9	1.3	2.1	3.1	2.65	3.1	2.6	1.8	0.92	0.66

performance of increasing the number of evaporators, operating three different storage systems, and operating an air-cooled condenser. The main findings are:

- The equivalent mechanical energy consumption of the optimized low-pressure plain MED process (10 effect) is 8 kWh/m^3, which is 59% lower than MED-TVC (with 7 effects). The optimal configuration reduces the solar field size by 25%. However, the heat transfer area increases by 128%.
- The cost analysis showed that at least 60% of the solar desalination plant capital costs are due to the solar field.
- By comparing three storage systems integrated with our plant, we found that the water storage system has 6% and 16% lower system capital costs compared with sensible heat storage and latent heat storage, respectively.
- The air-cooled condenser reduces water consumption by 2 m^3 of sea water per m^3 of feed. The performance of the air-cooled condenser is more sensitive to the sea water temperature than to the solar field size.
- Increasing the number of evaporators from 8 to 15 can reduce fan power by 21%. The monthly performance of the air-cooled condenser can vary by more than 300%, due to variations in dry bulb temperature and relative humidity.

Acknowledgments

This research was supported by a scholarship (210003978) from Hamad Bin Khalifa University (HBKU), a member of Qatar Foundation (QF). Any opinions, findings, and conclusions or recommendations expressed in this material are those of the author(s) and do not necessarily reflect the views of HBKU or QF. The authors would like to acknowledge Mr. Benjamin Figgis, Research Program Manager at the Qatar Environment and Energy Research Institute (QEERI), for providing the solar radiation data and the technical data for the linear Fresnel collector.

References

[1] A.M. Al Mutawa, N.A. Ruwaili, Waleed Mohamed Al Al Murbati, A.S. Al Oraifi, A. Al Oraifi, A. Al Arafati, A. Nasrullah, et al., Desalination in the GCC the history, the present & the future, 2014.
[2] Alhaj M, Mohammed S, Darwish M, Hassan A, Al-Ghamdi SG. A review of Qatar's water resources, consumption and virtual water trade. Desalin. Water Treat. 2017;90:70–85. http://dx.doi.org/10.5004/ dwt.2017.21246.
[3] Fichtner, MENA Regional Water Outlook Part II Desalination Using Renewable Energy, Germany, 2011. < http://www.medrc.org/download/twb/FICHT-6911691-v3-Task_1-Desalination_Potential.pdf > .
[4] Bamufleh H, Abdelhady F, Baaqeel HM, El-Halwagi MM. Optimization of multi-effect distillation with brine treatment via membrane distillation and process heat integration. Desalination 2017;408:110–8. http://dx.doi.org/10.1016/j.desal.2017.01.016.
[5] Carballo JA, Bonilla J, Roca L, De la Calle A, Palenzuela P, Alarcón-Padilla DC. Optimal operating conditions analysis for a multi-effect distillation plant according to energetic and exergetic criteria. Desalination 2018;435:70–6. http://dx.doi.org/10.1016/j.desal.2017.12.013.
[6] Shahzad MW, Burhan M, Ghaffour N, Ng KC. A multi evaporator desalination system operated with thermocline energy for future sustainability. Desalination 2018;435:268–77. http://dx.doi.org/10.1016/j.desal.2017.04.013.
[7] Mabrouk AA, Bourouni K, Abdulrahim HK, Darwish M, Sharif AO. Impacts of tube bundle arrangement and feed flow pattern on the scale formation in large capacity MED desalination plants. Desalination 2015;357:275–85. http://dx.doi.org/10.1016/j.desal.2014.11.028.
[8] Mabrouk AN, Fath HES. Technoeconomic study of a novel integrated thermal MSF–MED desalination technology. Desalination 2015;371:115–25. http://dx.doi.org/10.1016/j.desal.2015.05.025.
[9] Rahimi-Ahar Z, Hatamipour MS, Ghalavand Y. Solar assisted modified variable pressure humidification-dehumidification desalination system. Energy Convers. Manage. 2018;162:321–30. http://dx.doi.org/10.1016/j.enconman.2018.01.063.
[10] Palenzuela P, Alarcón-Padilla DC, Zaragoza G. Large-scale solar desalination by combination with CSP: techno-economic analysis of different options for the Mediterranean Sea and the Arabian Gulf. Desalination 2015;366:130–8. http://dx.doi.org/10.1016/j.desal.2014.12.037.
[11] El-Nashar AM. The economic feasibility of small solar MED seawater desalination plants for remote arid areas. Desalination 2001;134:173–86. http://dx.doi.org/10.1016/S0011-9164(01)00124-2.
[12] Palenzuela P, Hassan AS, Zaragoza G, Alarcón-Padilla D-C. Steady state model for multi-effect distillation case study: plataforma solar de almería MED pilot plant. Desalination 2014;337:31–42. http://dx.doi.org/10.1016/j.desal.2013.12.029.
[13] Askari IB, Ameri M. Techno economic feasibility analysis of Linear Fresnel solar field as thermal source of the MED/TVC desalination system. Desalination 2016;394:1–17. http://dx.doi.org/10.1016/j.desal.2016.04.022.
[14] Alarcón-Padilla DC, García-Rodríguez L, Blanco-Gálvez J. Experimental assessment of connection of an absorption heat pump to a multi-effect distillation unit. Desalination 2010;250:500–5. http://dx.doi.org/10.1016/j.desal.2009.06.056.
[15] M.T. Chaibi, A.M. El-Nashar, Solar thermal processes a review of solar thermal energy technologies for water desalination, in: G. Micale, L. Rizzuti, A. Cipollina (Eds.), Seawater Desalin. Conv. Renew. Energy Process., Springer Berlin Heidelberg, Berlin, Heidelberg, 2009, pp. 131–163. http://doi.org/10.1007/978-3-642-01150-4_6.
[16] Sharaf MA, Nafey AS, García-Rodríguez L. Exergy and thermo-economic analyses of a combined solar organic cycle with multi effect distillation (MED) desalination process. Desalination 2011;272:135–47. http://dx.doi.org/10.1016/j.desal.2011.01.006.
[17] Hamed OA, Kosaka H, Bamardouf KH, Al-Shail K, Al-Ghamdi AS. Concentrating solar power for seawater thermal desalination. Desalination 2016;396:70–8. http://dx.doi.org/10.1016/j.desal.2016.06.008.
[18] Iaquaniello G, Salladini A, Mari A, Mabrouk AA, Fath HES. Concentrating solar power (CSP) system integrated with MED–RO hybrid desalination. Desalination 2014;336:121–8. http://dx.doi.org/10.1016/j.desal.2013.12.030.
[19] A. Mabrouk, H. Fath, G. Iaquaniello, A. Salladini, Simulation and design of MED desalination plant with air cooled Condenser dirven by Concentrated Solar Power, in: Proc. IDA World Conf. Desalin. Water Sci. Int. Desalin. Assoc. World Congr. Desalin. Water, 2013.
[20] Mabrouk ANA, Fath HES. Experimental study of high-performance hybrid NF-MSF desalination pilot test unit driven by renewable energy. Desalin. Water Treat. 2013;51:6895–904. http://dx.doi.org/10.1080/19443994.2013.773860.
[21] Alhaj M, Hassan A, Darwish M, Al-Ghamdi SG. A techno-economic review of solar-driven multi-effect distillation. Desalin. Water Treat. 2017;90:86–98. http://dx.doi.org/10.5004/dwt.2017.21297.
[22] Alarcón-Padilla DC, García-Rodríguez L, Blanco-Gálvez J. Design recommendations for a multi-effect distillation plant connected to a double-effect absorption heat pump: a solar desalination case study. Desalination 2010;262:11–4. http://dx.doi.org/10.1016/j.desal.2010.04.064.
[23] P. Palenzuela, D.-C. Alarcón-Padilla, G. Zaragoza, Concentrating Solar Power and Desalination Plants, Spring International Publishing AG, 2015. http://doi.org/10.1007/978-3-319-20535-9.
[24] Stuber MD, Sullivan C, Kirk SA, Farrand JA, Schillaci PV, Fojtasek BD, et al. Pilot demonstration of concentrated solar-powered desalination of subsurface agricultural drainage water and other brackish groundwater sources. Desalination 2015;355:186–96. http://dx.doi.org/10.1016/j.desal.2014.10.037.
[25] Bataineh KM. Multi-effect desalination plant combined with thermal compressor driven by steam generated by solar energy. Desalination 2016;385:39–52. http://dx.doi.org/10.1016/j.desal.2016.02.011.
[26] Gholinejad M, Bakhtiari A, Bidi M. Effects of tracking modes on the performance of a solar MED plant. Desalination 2016;380:29–42. http://dx.doi.org/10.1016/j.desal.2015.11.015.
[27] V. Fulya, MENA Regional Water Outlook: Part II Desalination Using Renewable Energy, Stuttgart, Germany, 2011. https://doi.org/6543P07/FICHT-7109954-v2.
[28] Gude VG. Energy storage for desalination processes powered by renewable energy and waste heat sources. Appl. Energy 2015;137:877–98. http://dx.doi.org/10.1016/j.apenergy.2014.06.061.
[29] D. Alarcón, P. Fernández, Design and setup of a hybrid solar seawater desalination system : the aquasol project, in: Proc. ISES 2005 Sol. World Congr., International Solar Energy Society, Orlando, US, 2005.
[30] Kouta A, Al-Sulaiman F, Atif M, Bin Marshad S. Entropy, exergy, and cost analyses of solar driven cogeneration systems using supercritical CO_2 Brayton cycles and MEE-TVC desalination system. Energy Convers. Manage. 2016;115:253–64. http://dx.doi.org/10.1016/j.enconman.2016.02.021.

[31] Sharaf MA, Nafey AS, Garcia-Rodriguez L. Thermo-economic analysis of solar thermal power cycles assisted MED-VC (multi effect distillation-vapor compression) desalination processes. Energy 2011;36:2753–64. http://dx.doi.org/10.1016/j.energy.2011.02.015.
[32] Ghaffour N, Reddy VK, Abu-Arabi M. Technology development and application of solar energy in desalination: MEDRC contribution. Renew. Sustain. Energy Rev. 2011;15:4410–5. http://dx.doi.org/10.1016/j.rser.2011.06.017.
[33] Yılmaz İH, Söylemez MS. Design and computer simulation on multi-effect evaporation seawater desalination system using hybrid renewable energy sources in Turkey. Desalination 2012;291:23–40. http://dx.doi.org/10.1016/j.desal.2012.01.022.
[34] Mohamed SA, Al-Sulaiman FA, Ibrahim NI, Zahir MH, Al-Ahmed A, Saidur R, et al. A review on current status and challenges of inorganic phase change materials for thermal energy storage systems. Renew. Sustain. Energy Rev. 2017;70:1072–89. http://dx.doi.org/10.1016/j.rser.2016.12.012.
[35] Farid MM, Khudhair AM, Razack SAK, Al-Hallaj S. A review on phase change energy storage: materials and applications. Energy Convers. Manage. 2004;45:1597–615. http://dx.doi.org/10.1016/j.enconman.2003.09.015.
[36] Lane GA. Low temperature heat storage with phase change materials. Int. J. Ambient Energy 1980;1:155–68. http://dx.doi.org/10.1080/01430750.1980.9675731.
[37] A.M. Weiner, D.H. Blum, J.H.L. V, A.F. Ghoniem, Design of a hybrid RO-MED solar desalination system for treating agricultural drainage water in California, in: Proc. Int. Desalin. Assoc. World Congr. Desalin. Water Reuse, San Diego, California, USA, 2015.
[38] Industrial Solar thermal solutions GmbH, Technical Data Industrial Solar Fresnel collector LF-11, Freiburg, n.d.
[39] Schott Solar CSP GmBH, Schott PTR 70 Datasheet, Germany, n.d. < www.schott.com/csp > .
[40] H.T. El-Dessouky, H.M. Ettouney, Fundamentals of Salt Water Desalination, Elsevier, Amesterdam, 2002. https://doi.org/10.1016/B978-044450810-2/50008-7.
[41] Nayar KG, Sharqawy MH, Banchik LD, Lienhard V JH. Thermophysical properties of seawater: a review and new correlations that include pressure dependence. Desalination 2016;390:1–24. http://dx.doi.org/10.1016/j.desal.2016.02.024.
[42] Sharqawy MH, Lienhard JH, Zubair SM. Thermophysical properties of seawater: a review of existing correlations and data. Desalin. Water Treat. 2010;16:354–80. http://dx.doi.org/10.5004/dwt.2010.1079.
[43] Hassan AS, Darwish MA. Performance of thermal vapor compression. Desalination 2014;335:41–6. http://dx.doi.org/10.1016/j.desal.2013.12.004.
[44] Darwish M, Al-Juwayhel F, Abdulraheim H. Multi-effect boiling systems from an energy viewpoint. Desalination 2006;194:22–39.
[45] S. Kraemer, Commercializing Standalone Thermal Energy Storage, 2016.
[46] IEA-ETSAP, IRENA, Thermal Energy Storage Technology Brief, 2013. https://doi.org/10.1007/SpringerReference_7300.
[47] Qatar Meterology Department, Climatological Normals 1990–2013, 2018. < https://qweather.gov.qa/ClimateNormals.aspx > (accessed May 3, 2018).
[48] R.W. Hyland, A. Wexler, Formulations for the Thermodynamic Properties of the Saturated Phases of H2O from 173.15 K to 473.15 K, in: ASHRAE Trans., Washington, DC, 1983.
[49] J.A. Heyns, Performance characteristics of an air-cooled steam condenser incorporating a hybrid (dry/wet) dephlegmator, University of Stellenbosch, 2008.